Mechanistic Studies on Halo-Ligand Substitution of Five-Coordinate Trigonal-Bipyramidal Palladium(II) Complexes of Tris(2-(diphenylphosphino)ethyl)phosphine with Trimethyl Phosphite in Chloroform at Various Temperatures and Pressures

Sen-ichi Aizawa, Takashi Iida, and Shigenobu Funahashi*

Laboratory of Analytical Chemistry, Faculty of Science, Nagoya University, Chikusa, Nagoya 464-01, Japan

Received February 9, 1996[⊗]

Five-coordinate trigonal-bipyramidal palladium(II) complexes $[Pd(pp_3)X]X$ (pp_3 = tris(2-(diphenylphosphino)-ethyl)phosphine, $X^- = Cl^-$, Br^-, I^-) have been synthesized, and their structures in the solid state and in solution have been confirmed by X-ray crystal structure analysis and ^{31}P NMR spectroscopy, respectively. The ^{31}P NMR chemical shifts of the axial and equatorial phosphorus atoms indicate that the σ- and π-donating abilities of the axial monodentate ligands are in the order $Cl^- > Br^- > I^- \gg P(OCH_3)_3$. The thermodynamic parameters for the equilibria between the halo complexes, $[Pd(pp_3)Cl]^+ + X^- \rightleftarrows [Pd(pp_3)X]^+ + Cl^-$ ($X^- = Br^-$, I^-), have been determined as follows: $K^{298} = 1.70$, $\Delta H° = -5.66 \pm 0.07$ kJ mol^{-1}, and $\Delta S° = -14.6 \pm 0.2$ J K^{-1} mol^{-1} for Br^-; $K^{298} = 16.8$, $\Delta H° = -16 \pm 1$ kJ mol^{-1}, and $\Delta S° = -30 \pm 3$ J K^{-1} mol^{-1} for I^-. It is revealed that the relative stability of the halo complexes, $I^- > Br^- > Cl^-$ for the axial ligands, is determined by the difference in enthalpy. The second-order rate constants at 25 °C and activation parameters for the halo-ligand substitution with trimethyl phosphite, $[Pd(pp_3)X]^+ + P(OCH_3)_3 \rightarrow [Pd(pp_3)(P(OCH_3)_3)]^{2+} + X^-$ ($X^- = Cl^-$, Br^-, I^-), have been obtained as follows: $k^{298} = 1.19 \times 10^{-1}$ mol^{-1} kg s^{-1}, $\Delta H^‡ = 19 \pm 1$ kJ mol^{-1}, $\Delta S^‡ = -198 \pm 3$ J K^{-1} mol^{-1}, and $\Delta V^‡ = -25.5 \pm 0.5$ cm^3 mol^{-1} at 302.5 K for $X^- = Cl^-$; $k^{298} = 6.20 \times 10^{-2}$ mol^{-1} kg s^{-1}, $\Delta H^‡ = 23 \pm 3$ kJ mol^{-1}, $\Delta S^‡ = -191 \pm 3$ J K^{-1} mol^{-1}, and $\Delta V^‡ = -24.5 \pm 0.7$ cm^3 mol^{-1} at 302.5 K for $X^- = Br^-$; $k^{298} = 1.09 \times 10^{-2}$ mol^{-1} kg s^{-1}, $\Delta H^‡ = 57 \pm 4$ kJ mol^{-1}, $\Delta S^‡ = -89 \pm 15$ J K^{-1} mol^{-1}, and $\Delta V^‡ = -22.6 \pm 0.8$ cm^3 mol^{-1} at 302.9 K for $X^- = I^-$. The associative mechanism is proposed on the basis of the kinetic behavior and the activation parameters. The kinetic properties are discussed in terms of the electronic properties of the axial and entering ligands.

Introduction

The kinetics for ligand substitution reactions of metal complexes in solutions have been extensively investigated[1] because it is essential to clarify the reaction mechanism for metal complexes in order to understand their properties in solutions and in biological systems. So far, the kinetic properties of square-planar palladium(II) and platinum(II) complexes have been well established and the associative mechanism via a trigonal-bipyramidal transition state has been generally proposed.[1] In this mechanism, since the vacant nonbonding p_z orbital perpendicular to the square plane is able to accommodate an electron pair, an entering ligand may attack the vacancy.[2] On the other hand, because the d_{z^2} orbital is occupied, the entering ligand shifts to the equatorial plane to reduce the electronic repulsion and, consequently, pushes the leaving ligand away from the equatorial plane to form the trigonal plane in the transition state.[2]

In contrast with the square-planar complexes, the trigonal-bipyramidal complexes of d^8 metal ions have no vacant orbital. Therefore, the lone pair of the entering ligand exclusively brings about repulsive interaction with the occupied d orbitals in the associative mechanism. On the other hand, if the dissociative mechanism is promoted for the trigonal-bipyramidal complexes with the leaving ligand in the axial position, the bond-breaking energy is considerably large because of strong σ bonding with d_{z^2} orbital. Therefore, it is significant to investigate the substitution of the axial ligand in the trigonal-bipyramidal complexes. Though such studies can give us further insight into the kinetic properties of palladium(II) and platinum(II) complexes, so far there have been only a few mechanistic studies of trigonal-bipyramidal complexes of these metals.[3]

In the present work, we have selected the tripodal tetradentate ligand, tris(2-(diphenylphosphino)ethyl)phosphine (pp_3), as a bound ligand because the pp_3 ligand tends to form the trigonal-bipyramidal structure for the d^8 metal ions[4−8] and have synthesized the halo complexes $[Pd(pp_3)X]X$ ($X^- = Cl^-$, Br^-, I^-). We report the structural characterization of the halo complexes in the crystal form and in solution and the equilibria and kinetics for the axial monodentate-ligand substitution as the simple reaction for the mechanistic study of the trigonal-bipyramidal palladium(II) complexes. The present reuslts make it possible to compare the effects of the leaving halo ligands on the reaction mechanism.

Experimental Section

Reagents. Chloroform (Nakarai, Sp. Gr.), trimethyl phosphite (Wako, Sp. Gr.), deuterated chloroform ($CDCl_3$, Aldrich), and deuterated dichloromethane (CD_2Cl_2, Aldrich) were dried over activated 4A

[⊗] Abstract published in *Advance ACS Abstracts,* August 1, 1996.

(1) (a) Wilkins, R. G. *Kinetics and Mechanism of Reaction of Transition Metal Complexes,* 2nd ed.; VCH: Weinheim, Germany, 1991; Chapter 4. (b) Cross, R. J. In *Mechanisms of Inorganic and Organometallic Reactions*; Twigg, M. V., Ed.; Plenum: New York, 1988; Chapter 5.
(2) Lin, Z.; Hall, M. B. *Inorg. Chem.* **1991**, *30*, 646.
(3) (a) Meakin, P.; Jesson, J. P. *J. Am. Chem. Soc*. **1974**, *96*, 5751. (b) Pearson, R. G.; Muir, M. M.; Venanzi, L. M. *J. Chem. Soc*. **1965**, 5521.
(4) King, R. B.; Kapoor, R. N.; Saran, M. S.; Kapoor, P. N. *Inorg. Chem*. **1971**, *10*, 1851.
(5) Ghilardi, C. A.; Midollini, S.; Sacconi, L. *Inorg. Chem*. **1975**, *14*, 1970.
(6) Orlandini, A.; Sacconi, L. *Inorg. Chem*. **1976**, *15*, 78.
(7) Sacconi, L.; Dapporto, P.; Stoppioni, P.; Innocenti, P.; Benelli, C. *Inorg. Chem*. **1977**, *16*, 1669.
(8) Hohman, W. H.; Kountz, D. J.; Week, D. W. *Inorg. Chem*. **1986**, *25*, 616.

S0020-1669(96)00159-0 CCC: $12.00

Molecular Sieves and then distilled in a vacuum line. Tris(2-(diphenylphosphino)ethyl)phosphine (pp_3, Strem), bis(2-(diphenylphosphino)ethyl)phenylphosphine (p_3, Strem), and tetrakis(acetonitrile)-palladium(II) tetrafluoroborate (Aldrich) were used for the preparation of the palladium(II) complexes without further purification.

Preparation of Complexes. [Pd(pp_3)I]I. To a solution of $[Pd(CH_3CN)_4](BF_4)_2$ in acetonitrile was added a solution of an equimolar amount of pp_3 in dichloromethane, followed by concentrating the solution and keeping it in a refrigerator to give a pale yellow powder of $[Pd(pp_3)](BF_4)_2$.[9] To a suspension of $[Pd(pp_3)](BF_4)_2$ (1.42 g, 1.49 mmol) in a dichloromethane/nitromethane (5:1 v/v) mixture (60 cm^3) was added *n*-Bu_4NI (1.35 g, 3.66 mmol), whereupon the solution immediately turned from orange to deep red. The solution was concentrated to ca. 30 cm^3 and then kept in a refrigerator for 1 day. The resultant deep red crystals were collected by filtration and recrystallized from a dichloromethane/nitromethane (3:1 v/v) mixture. Yield: 90%. Single crystals were obtained by slow evaporation of a dichloromethane/nitromethane/acetonitrile solution and air-dried. Anal. Calcd for [Pd(pp_3)I]I: C, 48.93; H, 4.11; N, 0.00. Found: C, 46.75; H, 3.99; N, 0.36.

[Pd(pp_3)Br]Br. To a solution of $K_2[PdBr_4]$ (1.72 g, 3.41 mmol) in distilled water (10 cm^3) were added acetonitrile (80 cm^3) and a solution of pp_3 (2.52 g, 3.76 mmol) in chloroform (10 cm^3). The resultant red solution was separated into two phases by addition of water and chloroform. The chloroform phase was concentrated to obtain red crystals. Yield: 75%. This complex was also prepared by a procedure similar to that for [Pd(pp_3)I]I using *n*-Bu_4NBr instead of *n*-Bu_4NI. Yield: 75%. Single crystals were obtained by slow evaporation of an acetonitrile/water solution and air-dried. Anal. Calcd for [Pd(pp_3)Br]Br: C, 53.84; H, 4.52; N, 0.00. Found: C, 52.67; H, 4.71; N, 0.25.

[Pd(pp_3)Cl]Cl. The chloro complex was prepared by procedures similar to those for the bromo complex by using $K_2[PdCl_4]$ instead of $K_2[PdBr_4]$ and for the iodo complex by using *n*-Bu_4NCl instead of *n*-Bu_4NI. Yields: 89 and 80%, respectively. Single crystals were obtained from an acetonitrile/water solution and air-dried. Anal. Calcd for [Pd(pp_3)Cl]Cl: C, 59.49; H, 4.99; N, 0.00. Found: C, 56.84; H, 5.01; N, 0.15.

[Pd(pp_3)($P(OCH_3)_3$](BF_4)$_2$. The trimethyl phosphite complex was prepared by the procedure described previously.[9]

[Pd(p_3)X]X (X = Cl$^-$, Br$^-$, I$^-$). The square-planar complexes were prepared by procedures similar to those for the corresponding trigonal-bipyramidal complexes by using p_3 instead of pp_3. Anal. Calcd for [Pd(p_3)Cl]Cl: C, 57.27; H, 4.67; N, 0.00. Found: C, 57.20; H, 4.70; N, 0.00. Calcd for [Pd(p_3)Br]Br: C, 50.00; H, 4.15; N, 0.00. Found: C, 51.33; H, 4.20; N, 0.01. Calcd for [Pd(p_3]I]I: C, 45.64; H, 3.72; N, 0.00. Found: C, 44.54; H, 3.73; N, 0.04.

X-ray Structure Analysis. Each single crystal of chloro, bromo, and iodo complexes suitable for diffraction measurements was sealed in a 0.7 mm o.d. capillary tube without air-drying because acetonitrile molecules in the crystal are volatile to collapse the single crystal.[10] X-ray diffraction measurements were performed on a MAC Science Rapid X-Ray Diffraction Image Processor (DIP 320N) with graphite-monochromated Mo Kα radiation (λ = 0.710 73 Å) at ambient temperature. Reflections were collected by using 30 continuous Weissenberg photographs with a ϕ range of 6° (total ϕ range 0−180°). The intensity data were corrected for the standard Lorentz and polarization effects. An empirical absorption correction was not applied. The structures were solved by direct methods and refined by a full-matrix least-squares technique using Crystan-G (version 3).[11] All non-hydrogen atoms except for the carbon atoms for the iodo complexes were refined with anisotropic thermal parameters, and the hydrogen atoms were placed in the observed positions with fixed thermal parameters. The atomic scattering factors were taken from ref 12. The crystallographic data are summarized in Table 1. The crystallographic details, positional and thermal parameters for all atoms containing hydrogen atoms observed, and bond distances and angles for non-hydrogen atoms are listed in Tables S1−S4 (Supporting Information).

Table 1. Crystallographic Data for [Pd(pp_3)X]X·CH_3CN

X$^-$	Cl$^-$	Br$^-$	I$^-$
formula	$PdCl_2P_4NC_{44}H_{45}$	$PdBr_2P_4NC_{44}H_{45}$	$PdI_2P_4NC_{44}H_{45}$
fw	889.10	978.00	1072.00
a/Å	10.417(4)	10.470(3)	10.853(4)
b/Å	10.520(3)	10.482(5)	39.69(2)
c/Å	20.158(6)	20.37(1)	10.430(2)
α/deg	96.69(2)	103.53(2)	
β/deg	103.98(1)	96.53(4)	106.14(2)
γ/deg	104.86(2)	104.71(4)	
V/Å^3	2058(1)	2089(2)	4316(3)
Z	2	2	4
space group	*P*1 (No. 1)	*P*1 (No. 1)	$P2_1$ (No. 4)
T/K	295	295	295
λ/Å	0.710 73	0.710 73	0.710 73
ρ_{calc}/g cm^{-3}	1.45	1.58	1.65
μ/cm^{-1}	7.60	25.15	20.16
R^a	0.064	0.089	0.070
$R_w{}^b$	0.075	0.101	0.089

^{a} $R = \sum||F_o| - |F_c||/\sum|F_o|$. ^{b} $R_w = [\sum w(|F_o| - |F_c|)^2/\sum w|F_o|^2]^{1/2}$.

Measurements. The kinetic measurements for the substitution reactions of the chloro and bromo complexes with trimethyl phosphite in chloroform were carried out with a Shimadzu UV-265FW spectrophotometer. The measurements for the kinetics of the iodo complex and equilibria between halo complexes in deuterated chloroform were performed by ^{31}P NMR spectroscopy on a JEOL JMN-GX270 FT-NMR spectrometer operating at 109.3 MHz with sufficient acquisition time of at least 0.4 s. The substitution reactions at various pressures were followed spectrophotometrically by using a high-pressure static vessel equipped with a le Noble type quartz cell.[13] The temperature of the reaction solution was controlled within ±0.1 °C. Though about 15 min was required for the temperature and/or pressure equilibration, the reactions were sufficiently slow to obtain accurate rate constants. All sample solutions were prepared under a nitrogen atmosphere. Tetra-*n*-butylammonium bromide and iodide were used for the equilibrium measurements to adjust the concentration of the halide. Rates were measured under pseudo-first-order conditions where the concentrations of trimethyl phosphite were in large excess over the concentrations of the halo complexes. The leaving-ligand concentration dependence of the rates was checked by use of a large excess of tetra-*n*-butylammonium bromide for the bromo complex. The initial concentrations of the reactants for each kinetic and equilibrium measurements are given in Table S5 (Supporting Information).

Results and Discussion

Characterization. Each crystal of the halo complexes consists of two nonequivalent formula units, [Pd(pp_3)X]X·CH_3CN (X$^-$ = Cl$^-$, Br$^-$, I$^-$). The perspective views of the chloro, bromo, and iodo complexes are displayed in Figure 1a−c, respectively. The selected bond distances and angles are summarized in Table 2. The complex cations have a trigonal-bipyramidal geometry with the halo ligand and the central phosphorus atom of pp_3 in axial positions and the three terminal phosphorus atoms of pp_3 in equatorial positions. The halide counterions are located on sides opposite to the halo ligands. A significant difference in the structures of the Pd(pp_3) moieties is not observed among the halo complexes, though the Pd−X distances vary with the halide ion sizes. The average axial bond distance (Pd−P_{ax} = 2.22−2.23 Å) is notably shorter than the average equatorial bond distance (Pd−P_{eq} = 2.42−2.43 Å) for each complex. This is attributed to the strong σ interaction of

(9) Aizawa, S.; Funahashi, S. *Anal. Sci.* **1996**, *12*, 27.
(10) It was confirmed by X-ray analyses of the sealed crystals that one acetonitrile molecule was contained in each formula unit of the halo complexes while elemental analyses of the air-dried samples did not show the corresponding nitrogen content with reproducible values. The loss of the acetonitrile molecules from the crystals hindered our density measurements.
(11) Programs of a structure determination package from MAC Science, Yokohama, Japan, 1992.
(12) *International Tables for X-ray Crystallography*; Kynoch: Birmingham, England, 1974; Vol. IV.
(13) le Noble, W. J.; Schlott, R. *Rev. Sci. Instrum.* **1976**, *47*, 770.

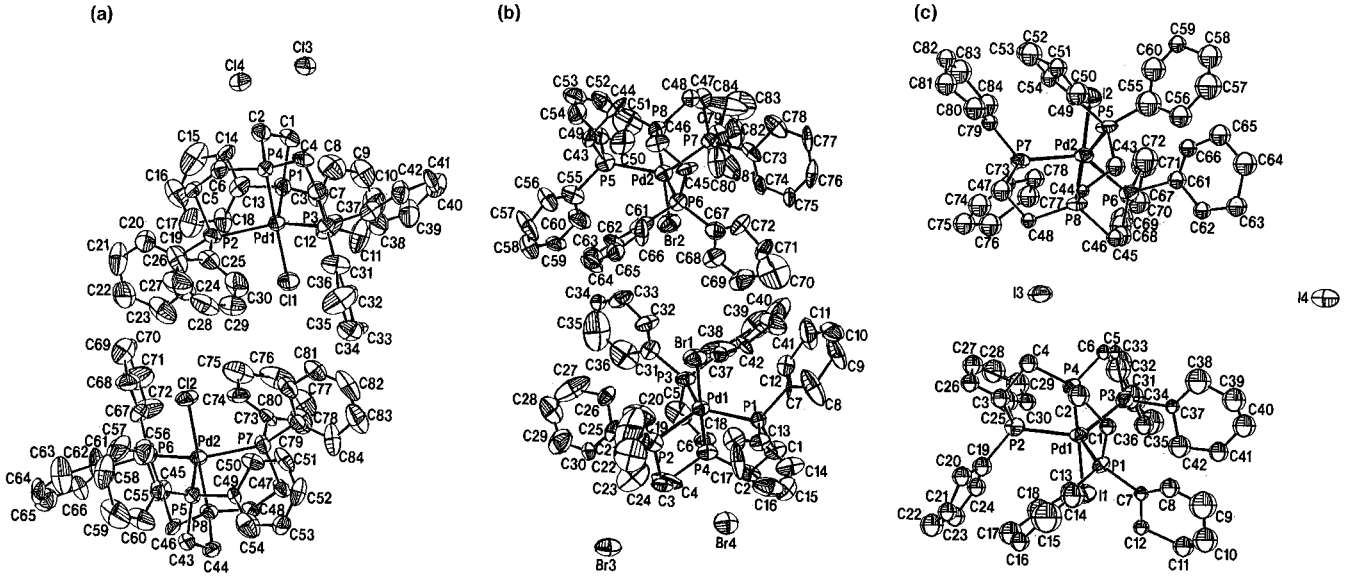

Figure 1. ORTEP diagrams for $[Pd(pp_3)X]X{\cdot}CH_3CN$ ($X^- = Cl^-$ (a), Br^- (b), I^- (c)). Acetonitrile molecules are omitted for clarity.

Table 2. Selected Bond Distances (Å) and Angles (deg) for $[Pd(pp_3)X]X{\cdot}CH_3CN$

$X^- = Cl^-$		$X^- = Br^-$		$X^- = I^-$	
Pd1−P1	2.436(4)	Pd1−P4	2.214(4)	I1−Pd1	2.690(2)
Pd1−P2	2.449(4)	Pd1−P1	2.389(6)	Pd1−P1	2.500(8)
Pd1−P3	2.388(4)	Pd1−P2	2.460(6)	Pd1−P2	2.373(9)
Pd1−P4	2.237(3)	Pd1−P3	2.462(5)	Pd1−P3	2.418(6)
Pd1−Cl1	2.414(4)	Pd1−Br1	2.516(2)	Pd1−P4	2.214(6)
Pd2−P5	2.446(4)	Pd2−P8	2.222(4)	I2−Pd2	2.684(3)
Pd2−P6	2.419(4)	Pd2−P5	2.386(6)	Pd2−P5	2.440(8)
Pd2−P7	2.456(4)	Pd2−P6	2.411(5)	Pd2−P6	2.420(6)
Pd2−P8	2.214(3)	Pd2−P7	2.412(6)	Pd2−P7	2.359(9)
Pd2−Cl2	2.422(3)	Pd2−Br2	2.519(2)	Pd2−P8	2.241(5)
P4−Pd1−P1	83.3(1)	P4−Pd1−P1	82.7(2)	P4−Pd1−P1	84.9(2)
P4−Pd1−P2	84.1(1)	P4−Pd1−P2	83.1(2)	P4−Pd1−P2	81.5(3)
P4−Pd1−P3	83.6(1)	P4−Pd1−P3	84.0(2)	P4−Pd1−P3	85.8(2)
P4−Pd1−Cl1	178.7(2)	P4−Pd1−Br1	178.0(2)	P4−Pd1−I1	176.4(3)
P1−Pd1−P2	113.3(1)	P1−Pd1−P2	121.9(2)	P3−Pd1−P1	113.4(3)
P1−Pd1−P3	121.4(1)	P1−Pd1−P3	121.7(2)	P3−Pd1−P2	123.6(3)
P1−Pd1−Cl1	98.0(1)	P1−Pd1−Br1	95.7(1)	P3−Pd1−I1	95.7(2)
P2−Pd1−P3	121.6(1)	P2−Pd1−P3	112.2(2)	P2−Pd1−P1	119.8(2)
P2−Pd1−Cl1	95.3(1)	P2−Pd1−Br1	98.7(1)	P2−Pd1−I1	95.0(2)
P3−Pd1−Cl1	95.7(2)	P3−Pd1−Br1	96.0(1)	P1−Pd1−I1	97.4(1)
P8−Pd2−P5	83.2(1)	P8−Pd2−P5	84.0(2)	P8−Pd2−P5	84.4(2)
P8−Pd2−P6	83.0(1)	P8−Pd2−P6	84.0(2)	P8−Pd2−P6	82.3(2)
P8−Pd2−P7	83.7(1)	P8−Pd2−P7	83.9(2)	P8−Pd2−P7	84.8(2)
P8−Pd2−Cl2	178.2(2)	P8−Pd2−Br2	178.2(2)	P8−Pd2−I2	177.5(2)
P5−Pd2−P6	121.0(1)	P5−Pd2−P6	121.8(2)	P7−Pd2−P5	120.6(2)
P5−Pd2−P7	113.5(1)	P5−Pd2−P7	121.2(2)	P7−Pd2−P6	124.0(3)
P5−Pd2−Cl2	98.5(1)	P5−Pd2−Br2	94.8(1)	P7−Pd2−I2	92.9(2)
P6−Pd2−P7	121.5(1)	P6−Pd2−P7	113.8(2)	P6−Pd2−P5	112.0(3)
P6−Pd2−Cl2	96.1(1)	P6−Pd2−Br2	95.5(1)	P6−Pd2−I2	98.2(1)
P7−Pd2−Cl2	95.5(1)	P7−Pd2−Br2	97.8(1)	P5−Pd2−I2	97.6(1)

the axial bond in the trigonal-bipyramidal geometry. A similar trend in difference in the axial and equatorial bond distances is observed for the analogous d^8 metal complexes $[Co(pp_3)(P(OCH_3)_3)]^+$ and $[Ni(pp_3)(P(OCH_3)_3)]^{2+}$.[8] The difference in the bond distances ($Co-P_{ax} = 2.125$ Å and $Co-P_{eq} = 2.211$ Å; $Ni-P_{ax} = 2.181$ Å and $Ni-P_{eq} = 2.275-2.325$ Å) is obviously smaller than that for the Pd(II) complexes, though the axial ligand, $P(OCH_3)_3$, trans to P_{ax} is a weaker σ donor compared to the halo ligands (vide infra). This finding indicates that the σ interaction of the phosphorus atom with the d^8 ions in the second-row transition metal series is relatively larger than that in the first-row transition metal series. For the present complexes, each Pd(II) ion is displaced by 0.25−0.28 Å from the equatorial plane defined by the three equatorial phosphorus atoms toward the halo ligand, and consequently, the chelate bite angles, $P_{ax}-Pd-P_{eq}$, are reduced to 83.5−84.0°. Since the distortion of the trigonal-bipyramidal structure does not depend on the size of the halo ligands, the chelate strain of the five-membered P−C−C−P chelate is expected.

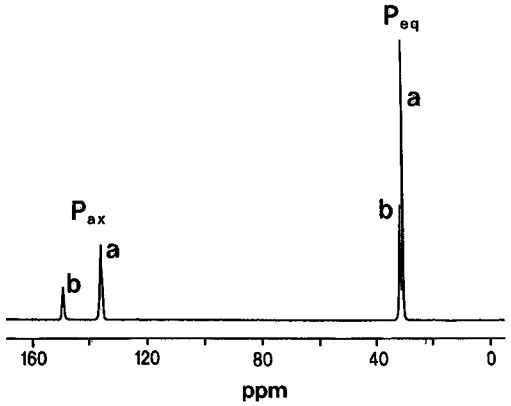

Figure 2. ^{31}P NMR spectra of the chloro (a) and iodo (b) complexes in the equilibrium in deuterated chloroform.

Table 3. ^{31}P NMR Chemical Shifts for the Halo and Trimethyl Phosphite Complexes[a]

complex	chemical shift/ppm[b]	
	P_{ax}	P_{eq}
$[Pd(pp_3)Cl]^+$	136.50	31.62
$[Pd(pp_3)Br]^+$	142.57	31.76
$[Pd(pp_3)I]^+$	147.35	31.98
$[Pd(pp_3)(P(OCH_3)_3)]^{2+}$	149.18[c]	43.48

[a] In deuterated dichloromethane. [b] Relative to 85% D_3PO_4 in D_2O. [c] Center of the doublet.

The ^{31}P NMR spectra of the halo complexes in deuterated chloroform and dichloromethane exhibit two peaks, the weaker peak in the lower field and the more intense peak in the upper field (Figure 2). The NMR spectra indicate that the halo complexes have trigonal-bipyramidal geometry at least with C_3 symmetry where the weaker and more intense peaks correspond to those for the central phosphorus atom in the axial position (P_{ax}) and the three equivalent terminal phosphorus atoms in the equatorial position (P_{eq}), respectively. The values of the ^{31}P NMR chemical shift in dichloromethane are listed in Table 3. The considerable lower field shift for P_{ax} compared with the chemical shift for P_{eq} is observed for each halo complex though

Table 4. Absorption Spectral Data for the Halo and Trimethyl Phosphite Complexes[a]

complex	transition energy/10^3 cm^{-1} (log(ϵ/M^{-1} cm^{-1}))	
	$^1A_1' \rightarrow {}^1E'$	$^1A_1' \rightarrow {}^1E''$
$[Pd(pp_3)Cl]^+$	20.75 (3.74 sh)	23.47 (3.85 sh)
$[Pd(pp_3)Br]^+$	20.37 (3.80 sh)	23.69 (3.90 sh)
$[Pd(pp_3)I]^+$	20.77 (3.80)	28.03 (4.03)
$[Pd(pp_3)(P(OCH_3)_3)]^{2+}$	24.10 (4.09 sh)	26.94 (4.32)

[a] In dichloromethane.

Table 5. Thermodynamic Parameters for the Equilibrium between $[Pd(pp_3)Cl]^+$ and $[Pd(pp_3)X]^+$ ($X^- = Br^-$, I^-)

X^-	K^{298}	$\Delta H°$/kJ mol^{-1}	$\Delta S°$/J K^{-1} mol^{-1}	$\Delta G°$/kJ mol^{-1} [a]
Br^-	1.70	-5.66 ± 0.07	-14.6 ± 0.2	-1.3 ± 0.1
I^-	16.8	-16 ± 1	-30 ± 3	-7.0 ± 2.1

[a] At 25 °C.

the equatorial terminal phosphorus atoms have two electron-withdrawing phenyl groups. This fact is consistent with the stronger σ donation from the axial phosphorus atom to the palladium(II) center as observed in the crystal structures. Furthermore, the electronic absorption spectra of $[Pd(pp_3)X]X$ ($X^- = Cl^-$, Br^-, I^-) and $[Pd(pp_3)(P(OCH_3)_3)](BF_4)_2$ in dichloromethane are compatible with those for the low-spin trigonal-bipyramidal complexes of d^8 metal ions.[14] The two absorption bands in the visible region for each complex are assigned to the transitions from $^1A_1'$ to $^1E'$ and $^1E''$ (Table 4).

As shown in Table 3, the ^{31}P NMR chemical shift is sensitive to the axially coordinated halo ligands. The order of the upfield shifts of P_{ax} and P_{eq} for $[Pd(pp_3)X]^+$ ($X^- = Cl^-$, Br^-, I^-) and $[Pd(pp_3)(P(OCH_3)_3)]^{2+}$ is $Cl^- > Br^- > I^- > P(OCH_3)_3$ for the axial ligands. The σ donation of the axial ligand weakens the σ Pd$-P_{ax}$ bond because of the competition for σ donation to the d_{z^2} orbital of the Pd(II) ion and, consequently, causes the shielding of the axial phosphorus atom. On the other hand, the π donation of the axial ligand increases the electron density in the d_{xz} and d_{yz} orbitals of the Pd(II) ion which have direct π interaction with the empty d orbitals of the equatorial phosphorus atoms. It should be mentioned that the influence of π donation of the axial ligand toward the axial phosphorus through the d_{xz} and d_{yz} orbitals is minor compared with that of the σ donation. Accordingly, the ^{31}P NMR chemical shifts for the present complexes demonstrate that the strengths of σ and π donations are both in the order $Cl^- > Br^- > I^- > P(OCH_3)_3$.

Equilibrium and Kinetics. It was confirmed by the ^{31}P NMR spectra that the equilibria, (1) and (2), between halo

$$[Pd(pp_3)Cl]^+ + Br^- \overset{K_1}{\rightleftharpoons} [Pd(pp_3)Br]^+ + Cl^- \quad (1)$$

$$[Pd(pp_3)Cl]^+ + I^- \overset{K_2}{\rightleftharpoons} [Pd(pp_3)I]^+ + Cl^- \quad (2)$$

complexes in deuterated chloroform were reached without any byproduct. The equilibrium constants, K_1 and K_2, were evaluated by the initial concentrations of the halo complexes and tetra-*n*-butylammonium halide and the relative intensity of the ^{31}P NMR signals for the axial phosphorus atoms of each halo complex in an equilibrium state which are well resolved (Figure 2). The temperature dependence of the equilibrium constants for each reaction is shown in Table S6 and Figure S1 (supporting information). The thermodynamic parameters obtained are listed in Table 5.

(14) Lever, A. B. P. *Inorganic Electronic Spectroscopy*, 2nd ed.; Elsevier: Amsterdam, 1984; Chapter 6.

Table 6. Activation Parameters for the Substitution Reactions of $[Pd(pp_3)X]^+$ ($X^- = Cl^-$, Br^-, I^-) with Trimethyl Phosphite in Chloroform

X^-	k^{298}/mol^{-1} kg s^{-1}	$\Delta H^{\ddagger}$/kJ mol^{-1}	$\Delta S^{\ddagger}$/JK^{-1} mol^{-1}	$\Delta V^{\ddagger}$/cm^3 mol^{-1}
Cl^-	11.9×10^{-2}	19 ± 1	-198 ± 3	-25.5 ± 0.5[a]
Br^-	6.20×10^{-2}	23 ± 1	-191 ± 3	-24.5 ± 0.7[a]
I^-	1.09×10^{-2}	57 ± 4	-89 ± 15	-22.6 ± 0.8[b]

[a] At 302.5 K. [b] At 302.9 K.

In process of the substitution reaction of halo complexes with trimethyl phosphite in deuterated chloroform (reaction 3), the

$$[Pd(pp_3)X]^+ + P(OCH_3)_3 \rightarrow [Pd(pp_3)P(OCH_3)_2]^{2+} + X^- \quad (X^- = Cl^-, Br^-, I^-) \quad (3)$$

^{31}P NMR peaks for the halo complexes and free trimethyl phosphite decreased as the peaks for the trimethyl phosphite complex[9] increased and the other peaks were not observed. The rates of the substitution reaction for the iodo complex were measured by the increase in peak height for the equatorial phosphorus atoms of the trimethyl phosphite complex under pseudo-first-order conditions. Since the substitution reactions for the chloro and bromo complexes are a little too fast to be followed by NMR measurements, the reactions were followed spectrophotometrically in chloroform solution. The isosbestic points in their spectral changes were observed at 324 and 403 nm for the bromo complex and at 321 and 401 nm for the chloro complex. The observed pseudo-first-order rate constants, k_{obs}, were determined by a least-squares analysis for the time course of the absorbance. The deviations of the k_{obs} values obtained at different wavelengths, 480, 440, and 350 nm, are less than $\pm 2\%$. Since the observed rate constants are proportional to the concentration of trimethyl phosphite as shown in Table S7 and Figure S2 (Supporting Information), reaction 3 is first order with respect to the entering-ligand concentration. The temperature dependence of the second-order rate constant, k, was fitted to the Eyring equation to give the values of activation enthalpy ($\Delta H^{\ddagger}$) and activation entropy ($\Delta S^{\ddagger}$) (Figure S3, Supporting Information). Since the plots of ln k vs pressure for the substitution reactions were linear within the experimental errors (Figure S4, Supporting Information), the values of activation volume ($\Delta V^{\ddagger}$) were determined from the slopes. All the activation parameters obtained are summarized in Table 6.

As apparent from the $\Delta G°$ values at 25 °C in Table 5, the relative stability of the halo complexes is in the order $I^- > Br^- > Cl^-$ for the axial halo ligands, and the order is determined by the difference in enthalpy. The contribution of entropy to the stability is in the reverse order because the larger halo ligand surrounded by the phenyl groups brings about more steric crowding. On the basis of the ^{31}P NMR chemical shifts, the enthalpic stabilization is attributable to the weakness of the π donation of the halo ligands rather than the strength of the σ donation. Such π interaction reduces the electronic repulsion between the occupied d_{xz} and d_{yz} orbitals and halo ligand and consequently strengthens the Pd$-$halo ligand bonding, while the σ donation of the halo ligands competitively weakens the σ bonding in the trans position.

We should consider some reaction mechanisms only on the basis of the good linearity of the entering-ligand concentration dependence of the pseudo-first-order rate constants. It has been confirmed that the pre-equilibrium with the dissociation of the halo ligand (mechanism I in Scheme 1) does not exist in the process of the substitution reaction from the fact that the reaction is not retarded by an increase in the halide ion concentration

Scheme 1

Mechanism I

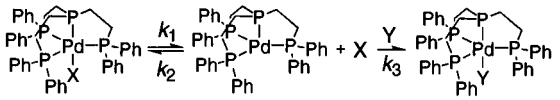

$$k_{obs} = \frac{k_1 k_3[Y]}{k_2[X] + k_3[Y]} \quad \text{If } k_2[X] >> k_3[Y],\ k_{obs} = \frac{k_1 k_3}{k_2[X]}[Y].$$

Mechanism II

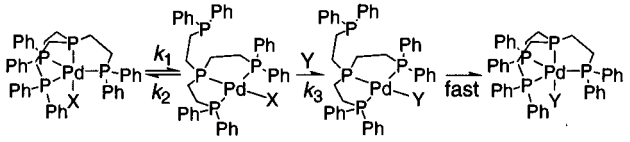

$$k_{obs} = \frac{k_1 k_3[Y]}{k_2 + k_3[Y]} \quad \text{If } k_2 >> k_3[Y],\ k_{obs} = \frac{k_1 k_3}{k_2}[Y].$$

Mechanism III

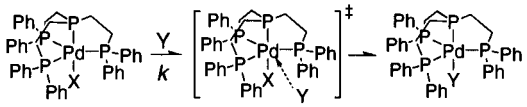

$$k_{obs} = k[Y]$$

(Table S7d). Judging from the much more negative values of $\Delta S^{\ddagger}$ and $\Delta V^{\ddagger}$ and relatively small values of $\Delta H^{\ddagger}$ for the present ligand substitution of the trigonal-bipyramidal Pd(II) complexes compared with those for the associative ligand substitution and solvent exchange of the square-planar Pd(II) complexes so far studied,[15] it is not probable that the square-planar intermediate is formed by the pre-equilibrium with the dissociation of one of the terminal diphenylphosphino groups (mechanism II in Scheme 1), because the first step in the dissociation should give positive entropy and volume changes and enthalpic destabilization due to bond cleavage.[16] Consequently, we can reasonably expect that the associative activation mode with the entering trimethyl phosphite attack on the trigonal-bipyramidal Pd(II) complex operates in the transition state (mechanism III in Scheme 1). Considering that trimethyl phosphite is a strong π acceptor and very weak σ donor, it is the most plausible that occupied d orbitals such as d_{xz} and d_{yz} of the Pd(II) ion interact with the empty d orbital of the phosphorus atom in trimethyl phosphite in the transition state and that the electronic repulsion between d orbitals of the Pd(II) ion and lone pair of the phosphorus atom is weak. A comparison of the activation parameters for the three halo complexes reveals that the reaction mechanism becomes more associative in the order $I^- < Br^- < Cl^-$ for the axial ligands. This order corresponds to that for the π-donating ability of the halo ligands which increase the electron density of the d_{xz} and d_{yz} orbitals and is advantageous to the interaction with the electron-accepting ligand. Therefore, the change in the activation parameters for the halo complexes supports the reaction mechanism proposed above. In addition, the distinguishably large negative $\Delta V^{\ddagger}$ values compared with those of the substitution reactions of the square-planar Pd(II) complexes[15] are due to the large void volume around the substitution site surrounded by the six phenyl groups which can accommodate the large volume of the entering ligand in the transition state.

Acknowledgment. This research was supported by Grants-in-Aid for Scientific Research (Nos. 06640779, 07454199, and 07504003) from the Ministry of Education, Science, and Culture of Japan. S.A. gratefully acknowledges receipt of a grant from the Kurata Foundation.

Supporting Information Available: X-ray crystallographic data (Table S1), atomic coordinates and isotropic thermal parameters (Table S2), anisotropic thermal parameters (Table S3), bond distances and angles (Table S4), initial compositions of the sample solutions for the kinetic and equilibrium measurements (Table S5), temperature dependences of the equilibrium constants (Table S6 and Figure S1), entering- and leaving-ligand concentration dependences of the observed rate constants (Table S7 and Figure S2), temperature dependences of the second-order rate constants (Table S8 and Figure S3), and pressure dependences of the second-order rate constants (Table S9 and Figure S4) (37 pages). Ordering information is given on any current masthead page.

IC9601596

(15) Kotowski, M.; van Eldik, R. In *Inorganic High Pressure Chemistry*; van Eldik, R., Ed.; Elsevier: Amsterdam, 1986; Chapter 4.

(16) We have obtained preliminary data for halo-ligand substitution reactions with trimethyl phosphite by using the corresponding square-planar halo complexes $[Pd(p_3)X]^+$ (p_3 = bis(2-(diphenylphosphino)-ethyl)phosphine; $X^- = Cl^-, Br^-, I^-$). The second-order rate constant at 25 °C (6.59×10^{-4} mol^{-1} kg s^{-1}) for the chloro complex obtained by the spectrophotometric method is much smaller than that for the corresponding five-coordinate complex in the present work under the same conditions (Table S7e). This fact is not consistent with mechanism II, Scheme 1, because k_1/k_2 should be much smaller than unity.